

Entanglement in non-equilibrium steady states and many-body localization breakdown through dissipative tunneling

Animesh Panda, and Sumilan Banerjee

Centre for Condensed Matter Theory, Department of Physics, Indian Institute of Science, Bangalore 560012, India

(Dated: November 22, 2022)

We model an electric-field or current driven interacting disorder system, coupled to environment at the boundaries, through an effective non-Hermitian Hamiltonian and study the entanglement properties of its eigenstates. In particular, we investigate whether a many-body localizable system undergoes a transition to a current-carrying non-equilibrium steady state under the drive and how the entanglement properties of the quantum states change across the transition. We also discuss the dynamics, entanglement growth, and long-time fate of a generic initial state under an appropriate time-evolution of the system governed by the non-Hermitian Hamiltonian. Our study reveals rich entanglement structures of the eigenstates of the non-Hermitian Hamiltonian. We find transition between current-carrying states with volume-law to area-law entanglement entropy, as a function of disorder and the strength of the non-Hermitian term, related to the dissipative tunneling to the environment.

Classification of many-body quantum states in terms of their entanglement properties has become a major endeavour in recent years in condensed matter physics. These activities have revealed intriguing connection of entanglement with dynamics and thermalization of quantum systems [1–3]. It has been found that typical high-energy eigenstates of a generic *isolated* many-body system can be classified as either *ergodic* or *many-body localized* (MBL) [4–6], based on whether the entanglement entropy of a subsystem scales as the volume [7] or the area of the subsystem, respectively. Starting with an un-entangled initial state, the MBL systems do not thermalize under the unitary dynamics, unlike the ergodic ones. However, the MBL systems still give rise to a slow growth of entanglement entropy approaching a state with sub-thermal volume law scaling [8–10]. One of the most natural realizations of MBL phases are found in strongly disordered systems where single-particle Anderson localization is stable to interaction [11–14], even at finite energy densities above the ground state.

However, condensed matter systems are seldom isolated. In particular, some very important experimental setups require the system to be connected with external environment. A prominent example is a system connected to leads and driven by current or a voltage bias or an electric field [see Fig.1(a)]. Generically, such systems are expected to attain an unique current-carrying non-equilibrium steady state (NESS). It is interesting to explore whether such NESSs could also be classified according to their entanglement content, e.g., a many-body localizable system undergoing an entanglement transition driven by a current or electric field. It is also important to ask whether the entanglement transition could be coincident with a transition between NESSs with and without current.

Recently there have been some studies of entanglement transition for the current carrying NESSs in non-interacting models using either scattering state [15, 16] or non-equilibrium Green's functions [17, 18]. Nevertheless, no known framework exist for studying entangle-

ment of driven states of a disordered interacting system connected to infinite leads at the boundaries. One possible way to access such boundary driven system is via Markovian Lindblad quantum master equation approximation [19, 20]. However, such Markovian evolution is destined to lead to a description of NESS in terms of mixed state having area law entanglement [21] and hence make the notion of entanglement transition obscure. An important avenue, at present, is to try to mimic such NESS in less microscopic *toy* models, e.g. boundary driven random unitary circuit model [15]. Here we take a different route, and try to address driven states of interacting disordered systems through an effective model which incorporates the boundary dissipation and the current drive via a non-Hermitian term.

We study the following non-Hermitian one-dimensional (1d) XXZ spin ($S = 1/2$) model with an uniform random field $h_i \in [-W, W]$, W being the disorder strength,

$$\mathcal{H} = -\frac{J}{2} \sum_i^L (e^{\Psi} S_i^+ S_{i+1}^- + e^{-\Psi} S_i^- S_{i+1}^+) - \sum_i^L h_i S_i^z - J_z \sum_i^L S_i^z S_{i+1}^z. \quad (1)$$

Here $S_i^\pm = (S_i^x \pm iS_i^y)$, L is the number of sites, Ψ is a real number (see below) and J, J_z are the spin exchanges; the latter controls the interaction strength. We apply periodic boundary condition. The above model can be rewritten as $\mathcal{H} = \mathcal{H}_h + i\lambda\mathcal{J}$, where \mathcal{H}_h is the usual Hermitian random field XXZ model with $J \rightarrow \tilde{J} = J \cosh \Psi$, $\lambda = J \sinh \Psi$ and $\mathcal{J} = -(iJ/2) \sum_i (S_i^+ S_{i+1}^- - S_i^- S_{i+1}^+)$ is the sum of spin current across the system.

The model can be mapped, via Jordan-Wigner transformation, to a model of fermions or hard-core bosons hopping on the 1d lattice with random disorder potential and nearest neighbour repulsion. In that case, Ψ is an imaginary vector potential through a ring [Fig.1(b)] and the model is an interacting version of Hatano-Nelson model [22–24]. The latter describes non-Hermitian

single-particle localization-delocalization transition. The fermion model is invariant under $\mathbf{i} = \sqrt{-1} \rightarrow -\mathbf{i}$, i.e. time (\mathcal{T}) reversal. However, as in the usual \mathcal{PT} -symmetric non-Hermitian models [25, 26], this \mathcal{T} - or pseudo \mathcal{PT} -symmetry can be broken by the eigenstates leading to complex eigenvalues. We refer to this real to complex transition as \mathcal{T} -reversal breaking for brevity even in the spin model [Eq.(1)]. Intriguingly, in the original Hatano-Nelson model the \mathcal{T} -symmetry breaking transition of the single-particle eigenstates coincides with the localization-delocalization transition and the delocalized states carry finite current. This leads to the question whether there is any *localization-delocalization* transition in the interacting model and whether the transition coincides with the \mathcal{T} -reversal breaking. Such congruence of the symmetry breaking and localization transition might lead to an exciting possibility of describing a “MBL transition” in terms of symmetry breaking.

Similar imaginary gauge potential, as in Eq.(1), has been also used in fermionic Hubbard model to describe electric-field driven Mott transition [27–29], where Ψ mimics the effect of dissipative tunneling to the environment [27]. In that case, the model has been shown [28] to describe many-body Landau-Zener (LZ) [30] quantum tunneling processes near field driven Mott transition within Dykhne [31] formalism. In this approach, a model with real gauge potential, such as for a constant electric field, is analytically continued to imaginary gauge potential to describe LZ transition. It is an interesting question whether such many-body LZ processes could provide an effective description for field or current driven transition in a MBL system. Here we do not attempt to address this issue, and, instead, use the non-Hermitian model [Eq.(1)] as an effective model to generate current driven pure states and describe possible entanglement transitions among them.

We further extend the model of Eq.(1) to describe the approach to the long-time NESS through the following dynamical equation for density matrix ρ ,

$$\frac{d\rho}{dt} = -i[\mathcal{H}_h, \rho] + \lambda(\{\mathcal{J}, \rho\} - 2\text{Tr}(\rho\mathcal{J})) \equiv \mathcal{L}\rho. \quad (2)$$

Here \mathcal{L} defines a Liouvillian operator. The above model has been used previously in the context of \mathcal{PT} -symmetric quantum mechanics to describe system with gain and loss [32]. Similar model has been also used in the context of field-driven Mott transition [29]. Eq.(2) can describe the evolution of both pure and mixed states and keep $\text{Tr}\rho(t) = 1$. Unlike in a Lindblad master equation, an initial pure state remains pure during the time evolution, and, in this case, Eq.(2) reduces to a complex Schrodinger equation [32]. From Eq.(2), $\rho(t)$ can be formally written using the non-Hermitian Hamiltonian [Eq.(1)] as $\rho(t) = e^{-i\mathcal{H}t} \rho_0 e^{i\mathcal{H}^\dagger t} / \text{Tr}(e^{-i\mathcal{H}t} \rho_0 e^{i\mathcal{H}^\dagger t})$, where ρ_0 is the initial density matrix. In particular, for an initial pure state $\rho_0 = |\psi\rangle\langle\psi|$, the state at time t is given

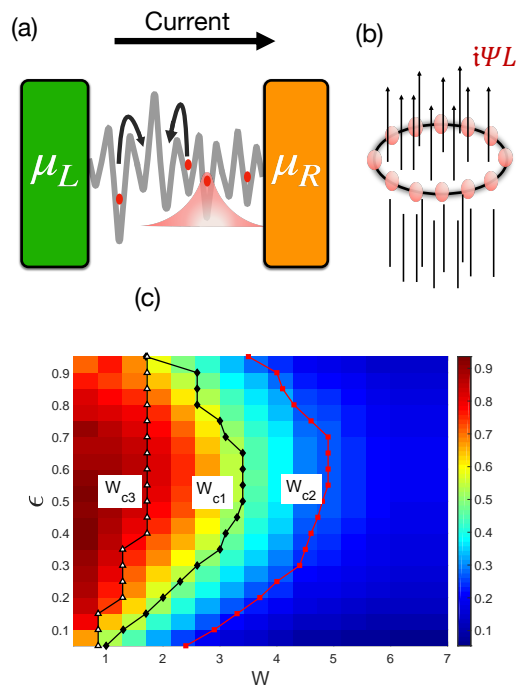


FIG. 1. **The model and the phase diagram:** (a) Schematic of an interacting disordered system driven by current through a voltage bias, $\mu_R - \mu_L$, applied between left and right leads with chemical potentials μ_L and μ_R , respectively. (b) The non-Hermitian model [Eq.(1)] mapped to fermions hopping on a ring with an imaginary flux $i\Psi L$. (c) The phase diagram for $\Psi = 0.3$. Eigenstates have volume-law entanglement and are delocalized for $W < W_{c1}$, whereas, for $W > W_{c1}$, states have area-law entanglement and are localized. The color indicates the slope of the participation entropy with the system size. A finite fraction of eigenstates breaks \mathcal{T} -reversal for $W < W_{c2}$. The region, $W_{c1} < W < W_{c2}$, have area-law localized states that break \mathcal{T} -reversal. There is a separate transition at W_{c3} in terms of system-size scaling of current (see main text).

by

$$|\psi(t)\rangle = \frac{\sum_n e^{-i\mathcal{E}_n t + \Lambda_n t} \langle n_L | \psi \rangle |n_R\rangle}{|\sum_n e^{-i\mathcal{E}_n t + \Lambda_n t} \langle n_L | \psi \rangle |n_R\rangle|} \quad (3)$$

Here $|n_L\rangle$ and $|n_R\rangle$ are the left and right eigenvectors of \mathcal{H} with eigenvalue $E_n = \mathcal{E}_n + i\Lambda_n$ and the left and right eigenvectors form an orthonormal basis, $\langle n_L | m_R \rangle = \delta_{nm}$ and $\sum_n |n_L\rangle\langle n_R| = \mathbb{I}$. The real part of the eigenvalue $\mathcal{E}_n = \langle n_R | \mathcal{H}_h | n_R \rangle / \langle n_R | n_R \rangle$, i.e. the expectation of parent Hermitian Hamiltonian, and the imaginary part $\Lambda_n \propto \mathcal{J}_n = \langle n_R | \mathcal{J} | n_R \rangle / \langle n_R | n_R \rangle$. It can be easily shown from Eq.(3) that, for eigenspectrum with non-zero imaginary part of the eigenvalues, the NESS $|\psi_\infty\rangle \equiv |\psi(t \rightarrow \infty)\rangle$ is given by $|\psi_\infty\rangle = (\langle s_L | \psi \rangle / |\langle s_L | \psi \rangle|) (|s_R\rangle / |\langle s_L | \psi \rangle|)$ where $|s_L\rangle$ is the eigenvector with maximum imaginary part of the eigenvalue Λ_s . We obtain the eigenvalues and the (left and right) eigenvectors of the non-Hermitian Hamiltonian [Eq.(1)] using numerical exact diagonalization for

system sizes $L = 10 - 16$ and sample over many disorder realizations (10000 for $L = 10$, 6000 for $L = 12$, 1440 for $L = 14$, and 200 for $L = 16$). The Hamiltonian [Eq.(1)] and the dynamics [Eq.(2)] conserves $S_z^{tot} = \sum_i S_i^z$. Hence we work in the $S_z^{tot} = 0$ subspace. We take the interaction $J_z = J = 1$ and vary W and Ψ .

We construct the phase diagram [Fig.1(c)] for the model [Eq.(1)] as a function of the disorder (W) and the quantity, $\epsilon = (\mathcal{E} - \mathcal{E}_0)/(\mathcal{E}_M - \mathcal{E}_0)$, defined from the real part of the eigenvalues; \mathcal{E}_M and \mathcal{E}_0 are the maximum and the minimum values of \mathcal{E} , respectively. For brevity, we refer to ϵ as *energy density*. We characterize the phases based on the finite-size scaling of the entanglement entropy, \mathcal{T} -symmetry breaking of the eigenstates and the current $j_n = \mathcal{J}_n/L$. Based on the dynamics defined in Eq.(2), we also look into the long-time steady state and the time-evolution of entanglement entropy starting from an initially un-entangled state. Our main results are as follows –

(1) We find a transition, $W_{c1}(\epsilon)$, from a volume-law to an area-law entangled phase as a function of W and ϵ . As in the usual MBL transition, we find the entanglement transition to coincide with Hilbert-space delocalization-transition. The entanglement transition moves to higher disorder with increasing strength of the non-Hermitian term (Ψ). In this sense, a non-zero Ψ causes a *breakdown* of the MBL states of the parent Hermitian model.

(2) We obtain a separate boundary, $W_{c2}(\epsilon)$, for \mathcal{T} -symmetry breaking transition. Hence, unlike the non-interacting case [22, 24], the localization transition does not coincide with \mathcal{T} -reversal symmetry breaking.

(3) We find yet another distinct transition $W_{c3}(\epsilon)$, within the \mathcal{T} -reversal broken region in terms of the scaling of the current j_n 's with system size.

(4) As in the Hermitian MBL systems, the entanglement entropy in the volume-law phase grows linearly with t . In contrast, both in the \mathcal{T} -reversal broken and unbroken area-law phase, entanglement entropy grows as $\ln(t)$. However, the entanglement growth is followed by a decay at late times towards a unique NESS.

(5) We find that the memory of the initial state, characterized in terms of an order parameter, gets eventually lost as the NESS is attained at long times.

Hilbert-space delocalization-localization transition: To characterize the eigenstates of the non-Hermitian Hamiltonian [Eq.(1)], we first obtain a phase diagram in terms a diagnostic of Hilbert-space localization, namely the participation entropy, $S_P(|n_R\rangle) = -\sum_\alpha p_\alpha^{(n)} \ln p_\alpha^{(n)}$ of the eigenstates in the basis of the spin configurations, $|\alpha\rangle = |S_1^z, S_2^z, \dots, S_N^z\rangle$ [33, 34] with $p_\alpha^{(n)} = |\langle \alpha | n_R \rangle|^2$. In the delocalized phase, $S_P = a \ln D_H$, where $a \approx 1$ and D_H is the dimension of the Hilbert space. On the other hand, in the localized phase, $a \approx 0$, and instead, one expects $S_P \sim \ln(\ln D_H)$ [34]. We obtain the disorder averaged $S_P(\epsilon)$ as a function W and ϵ [Fig.1] for $\Psi = 0.3$ and $L = 16$. Indeed, as in the Hermitian MBL case [34, 35], we find a delocalization-transition. The transition shifts to higher disorder for increasing Ψ (see the

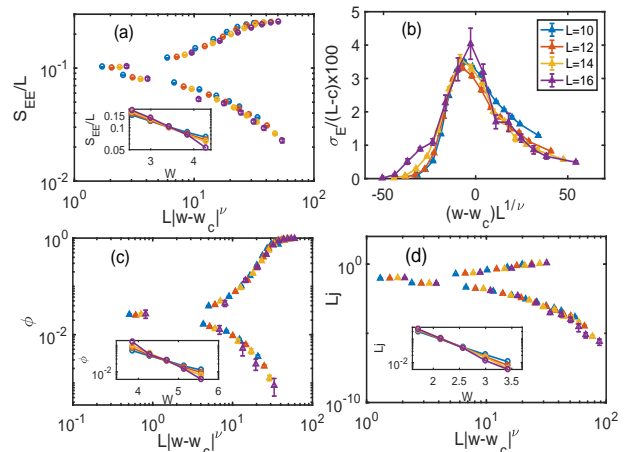


FIG. 2. **Entanglement and \mathcal{T} -reversal breaking transitions:** Finite-size scaling collapses for $\Psi = 0.3$ at energy density $\epsilon = 0.5$: (a) the entanglement entropy S_{EE} , (b) variance of entanglement entropy σ_E , (c) fraction of imaginary eigenvalues ϕ , and (d) the average current j . The transitions are detected from the crossing of the curves, as shown in the insets of (a) for S_{EE}/L , (c) for ϕ , and (d) for Lj , as a function W for different L . The values of the critical exponents and critical disorder extracted for the three transitions are, (a) $\nu_1 \simeq 1$, $W_{c1} = 3.6 \pm 0.1$, (c) $\nu_2 \simeq 0.9$, $W_{c2} = 4.75 \pm 0.1$ and (d) $\nu_3 \simeq 1.0$, $W_{c3} = 2.3 \pm 0.10$; c is a fitting parameter in (b) (see main text).

Supplementary Material (SM) [35], S1).

Entanglement transition: Next, we obtain the von Neumann entanglement entropy S_{EE} for each the eigenstates, i.e. $S_{EE}(|n_R\rangle) = -\text{Tr}(\rho_A \ln \rho_A)$. Here $\rho_A = \text{Tr}_B |n_R\rangle\langle n_R|$ is the reduced density matrix of the subsystem A , for the real-space bipartition of the system into left half, A , and right half, B . For $\Psi = 0.3$, the disorder averaged S_{EE} is plotted for $\epsilon = 0.5$, at the middle of the spectrum, as a function of W for different system sizes in Fig.2(a)(inset). We find a clear crossing of the S_{EE}/L vs. W curves around $W = W_{c1} \approx 3.6$, implying an entanglement transition, similar to the Hermitian case [34, 35]. The dependence of S_{EE} on L is consistent with a volume-law scaling for $W < W_{c1}$, and an area-law scaling for $W > W_{c1}$ (SM [35], S2). The transition is further corroborated by a reasonably good data collapse [Fig.2(a)], obtained using the finite-size scaling ansatz $S_{EE}(L) = Lg(L^{1/\nu_1}(W - W_{c1}))$ [34], where $g(x)$ is the scaling function. We find a critical exponent $\nu_1 \simeq 1$ and $W_{c1} \simeq 3.6$ from the scaling collapse. The crossing of the curves and the data collapse are most prominent near the middle of the spectrum. For a larger value of $\Psi = 0.6$, we find $W_{c1} = 4.2 \pm 0.1$, and $\nu_1 = 1.5$, i.e the extracted critical exponent changes with Ψ (see SM [35], S21) [36].

We obtain the phase boundary [Fig.1(b)] from the standard deviation, σ_E , of the entanglement entropy over disorder realizations. At the transition, σ_E is expected to show a peak that diverges with L [37]. In Fig.2(b), we

obtain a data collapse of $\sigma_E/(L-c)$ vs. W for $\Psi = 0.3$ and $\epsilon = 0.5$ with c as a fitting parameter [34] and the values of ν_1 and W_{c1} obtained from the finite-size scaling of S_{EE} . We plot a phase boundary in the $W - \epsilon$ plane for the entanglement transition from the peak position of σ_E for $L = 16$. The phase boundary is consistent with that obtained from the participation entropy [Fig.1(c)].

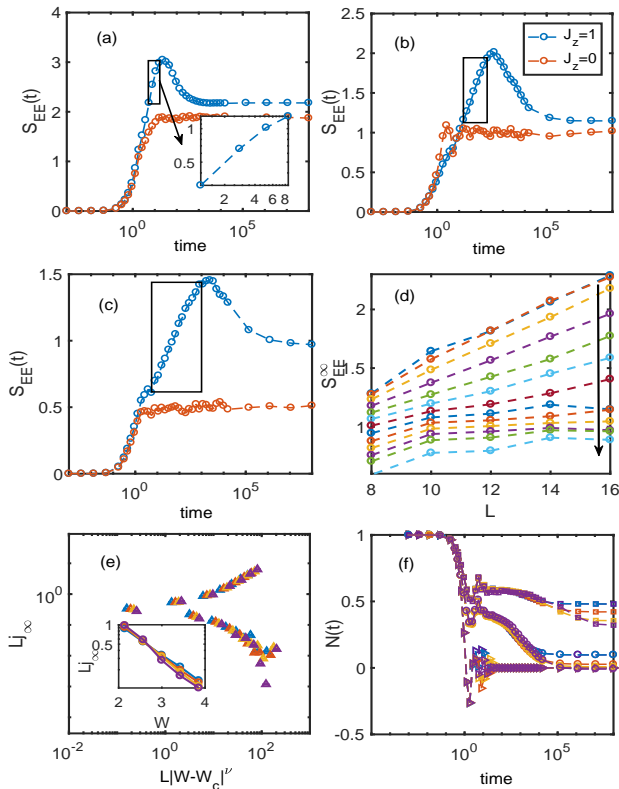


FIG. 3. Time evolution and NESS: (a)-(c) Semilog plots of entanglement entropy S_{EE} vs. t for $W = 2.15, 4.3, 5.57$, respectively, starting with the Ne'el state, for the interacting, $J_z = 1$ ($S_{EE}^{J_z=1}$), and the non-interacting cases, $J_z = 0$ ($S_{EE}^{J_z=0}$). Inset in (a) shows log-log plot of $S_{EE}^{J_z=1}(t) - S_{EE}^{J_z=0}(t \rightarrow \infty)$ vs. t . The boxes in (b), (c) indicate the initial logarithmic growths in the localized phases, with and without \mathcal{T} -reversal breaking, respectively. (d) Entanglement entropy, S_{EE}^∞ , of the long-time NESS, as a function of L for different W ; the arrow indicates increasing values of $W = 1.6 - 6$, equally spaced, and $W = 7$. (e) Finite-size scaling collapse of long-time steady state current j_∞ with $W_c = 2.9 \pm 0.1$ and $\nu = 1.8$. Inset shows the transition in terms of crossing of Lj_∞ vs. W curves for different L , in a semilog plot. (f) Time evolution of Ne'el order parameter as a function of W and L . The triangles, circles and squares are for $W = 0.43, 4.3, 7$, respectively, with $L = 10$ (blue), $L = 12$ (orange), $L = 14$ (yellow) and $L = 16$ (purple).

\mathcal{T} -reversal breaking: We now address the question whether the entanglement or the localization transition coincides with the \mathcal{T} -reversal breaking, as in the non-interacting model [22–24]. We define a \mathcal{T} -reversal order

parameter, $\phi(\epsilon)$, the fraction of imaginary eigenvalues at ϵ . We find a clear crossing of the ϕ vs. W curves for different L , as shown in Fig.2(c) (inset) for $\Psi = 0.3$ and $\epsilon = 0.5$. However, as evident, the crossing point is at $W = W_{c2} \approx 4.75$, clearly larger than W_{c1} for the entanglement transition. A good scaling collapse can again be obtained with an exponent $\nu_2 \simeq 0.9$ and $W_{c2} = 4.75 \pm 0.1$ [Fig.2(c)]. The collapse of the data for ϕ vs. W could not be obtained with $W_{c2} = W_{c1}$. This establishes the fact that \mathcal{T} -reversal breaking is distinct from the entanglement transition and occurs within the area-law phase. We find similar results for $\Psi = 0.6$ (see SM [35], S21), namely $W_{c2} = 5.6 \neq W_{c1}$. In this case, the critical exponent $\nu_2 = 1.5$. From the crossing points of $\phi(\epsilon)$ vs. W curves we obtain the phase boundary for the \mathcal{T} -reversal breaking in Fig.1(c).

To further characterize the \mathcal{T} -reversal breaking eigenstates, we compute the current $j(\epsilon)$, obtained by averaging over the magnitude of the currents, $|j_n|$, carried by the eigenstates with imaginary eigenvalues, and disorder realizations. Again, we find a crossing ($W = W_{c3} \approx 2.3$) in the $\mathcal{J} = Lj$ vs. W plots for different L [Fig.2(d)] at $\epsilon = 0.5$ for $\Psi = 0.3$. The transition, which we refer to as *current transition* for brevity, is seemingly distinct from both entanglement and \mathcal{T} -reversal breaking transitions. We can obtain a scaling collapse for j with $\nu_3 = 1$ and $W_{c3} = 2.3$, as shown in Fig.2(d)(inset). We obtain a phase boundary for the current transition at other values of ϵ from the crossing points, as shown in Fig.1(c).

The scaling of j with L for $W \ll W_{c3}$ is consistent with j approaching a constant for $L \rightarrow \infty$ (not shown). The scale-invariant crossing point indicates a diffusive scaling of the current at the transition, namely $j \sim 1/L$. In fact, for $W_{c3} < W \lesssim W_{c2}$, the scaling of j with L could be consistent with $j \sim 1/L^\gamma$ with $\gamma \gtrsim 1$, and we expect $j \sim e^{-L/\zeta}$ for $W \gg W_{c2}$, deep inside the \mathcal{T} -reversal unbroken localized phase; ζ is the characteristic localization length. However, this is hard to verify from the exact diagonalization numerics limited to such small system sizes. As discussed later [see Fig.3(d)], the current, j_∞ , carried by the long-time NESS also exhibits similar transition. For $W > W_{c1}$, in the area-law phase, the scaling of the current and the transition at W_{c2} could be studied by a matrix-product operator (MPO) based implementation [19, 20] of the dynamical evolution in Eq.(2). It would be interesting to establish the existence of such current-carrying pure NESS with area-law entanglement in an interacting system, as discussed in ref.[15].

Growth and decay of entanglement entropy and the approach to NESS: We study the time-evolution of the Ne'el state $|\psi_0\rangle = |\uparrow\downarrow\uparrow\downarrow \dots\rangle$ using Eq.(3). We compute the entanglement entropy, $S_{EE}(t)$, as function of time from the time-evolved state $|\psi(t)\rangle$ [Eq.(3)]. The results for $S_{EE}(t)$ are shown in Figs.3(a)-(c) for three values of disorder strength, (a) $W = 2.15$, in the volume-law phase, (b) $W = 4.3$, the \mathcal{T} -reversal broken area-law phase, and (c) $W = 5.57$, the \mathcal{T} -reversal unbroken area-law phase. In each of the cases, to bring out the cru-

cial effect of interaction, we compare $S_{EE}(t)$ with that obtained for the non-interacting Hatano-Nelson model ($J_z = 0$). The prominent features of $S_{EE}(t)$ are, (a) an initial growth, (b) a broad peak followed by a decay or relaxation, and (c) an eventual approach to a steady state value corresponding to the NESS. In the volume-law phase [Fig.3(a)(inset)], $S_{EE}(t)$ grows linearly with time, whereas, $S_{EE}(t) \propto \ln t$ initially in the area-law phases [Fig.3(b)-(c)], as in the Hermitian MBL case [8].

Using Eq.(3), the growth and subsequent decay of entanglement entropy can be understood from the density matrix, $\rho(t) = |\psi(t)\rangle\langle\psi(t)| = e^{-\mathcal{L}t}\rho_0 = \sum_{n,m} e^{-(\beta_{nm} + i\delta_{nm})t} C_{nm}^\psi(t) |n_R\rangle\langle m_R|$, where the coefficient $C_{nm}^\psi(t)$ is obtained from Eq.(3). Here $-(\beta_{nm} + i\delta_{nm})$ could be thought of as the eigenvalues of the Liouvillian operator \mathcal{L} ; $\beta_{nm} = 2\Lambda_s - \Lambda_n - \Lambda_m \geq 0$ and $\delta_{nm} = \mathcal{E}_n - \mathcal{E}_m$. The real part, $-\beta_{nm}$, of eigenvalue of \mathcal{L} leads to relaxation and $\beta_{nm} = 0$ corresponds to the long-time steady state. For weak-strength ($\Psi \ll 1$) of the non-Hermitian term, and for $t \ll e^L$ [38], $\delta_{typ} \gg \beta_{typ}$, and the initial growth of the entanglement entropy appears over a time window, $\delta_{typ}^{-1} \lesssim t \lesssim \beta_{typ}^{-1}$, due to the dephasing from the exponential factor $e^{i\delta_{nm}t}$ in $\rho(t)$. In this time window, the factor $e^{-\beta_{nm}t} \approx 1$. Here δ_{typ} and β_{typ} are the typical values of δ_{nm} and β_{nm} , respectively, that contributes to $\rho(t)$ for $t \ll e^L$.

This initial dephasing mechanism is similar to the one that leads to $\ln t$ -growth of entanglement entropy in the MBL phase [9]. For the interacting system, left to itself, the dephasing would typically lead to a diagonal ensemble and long-time state with volume-law entanglement, as it does for the MBL phase [8]. Nevertheless, for the non-Hermitian case, the relaxation due to β_{nm} kicks in for $t \gtrsim \beta_{typ}^{-1}$ and gives rise to the decay of $S_{EE}(t)$, as in Fig.3(a)-(c), before the system could reach the diagonal ensemble. However, β_{nm} is expected to have gap [39], $\beta_g \sim \mathcal{O}(1)$, above its minimum value, $\beta_{nm} = 0$ (see SM [35], S31). On the contrary, the spectrum of δ_{nm} is gapless, $\min(\delta_{nm}) \sim e^{-L}$. Hence, there could be interesting dephasing dynamics that goes on during the decay over $\beta_{typ}^{-1} \lesssim t \lesssim \beta_g^{-1}$, even though $\delta_{typ} \gg \beta_{typ}$. For $t > \beta_g^{-1}$, the entanglement entropy rapidly approaches the value for that of the NESS, dictated by the eigenstate with the maximum imaginary part for the eigenvalue, as discussed earlier.

We have also studied the system-size scaling of S_{EE}^{peak} , the maximum value of $S_{EE}(t)$ in Figs.3(a)-(c), as well as that of $S_{EE}^\infty = S_{EE}(t \rightarrow \infty)$, the entanglement entropy of the NESS. As shown in Fig.3(d) and in the SM [35],

S32, we find no volume-law to area-law transition in either S_{EE}^{peak} or S_{EE}^∞ with the disorder strength. In fact, S_{EE}^{peak} and S_{EE}^∞ neither scale as the volume nor the area, even though both of these increase with L (see SM [35], S32).

As already discussed, there is also a current transition for the NESS, as in Fig.2(d) for the eigenstates. The transition is shown in terms of a finite-size scaling collapse for Lj_∞ vs. W curves in Fig.3(e). We also show the time-evolution of Ne'el order parameter $N(t) = (2/L) \sum_i (-1)^i \langle \psi(t) | S_i^z | \psi(t) \rangle$ in Fig.3(f). This characterizes the memory of the initial state and approaches a finite value for $t \rightarrow \infty$ for the infinite system size in the MBL phase; $N(t)$ decays to zero with time in the ergodic phase. Here, for the non-Hermitian case, we find that $N_\infty = N(t \rightarrow \infty)$, i.e. the Neel order of the NESS, decreases with L , even for strong disorder, deep in the area-law phase. This is expected in a driven system, which loses its initially memory due to the drive. We also notice an interesting dynamical regime, presumably over the time window $\beta_{typ}^{-1} < t < \beta_g^{-1}$, in the decay of $N(t)$ [Fig.3(f)]. The order parameter plateaus over a region as a function of t , as if trying to retain the initial memory. In contrast, such regime is absent in the Hermitian model (see SM [35], S33).

In conclusion, we have studied a non-Hermitian disordered model, the interacting version of Hatano-Nelson model [22]. We propose that the model can be used to generate various current-carrying states and study there entanglement properties. We have established a rich phase diagram based on the properties of the eigenstates and the long-time NESS, as well as, from the time evolution of entanglement entropy, as a function of disorder. In future, it would be interesting verify whether the non-Hermitian model can indeed describe some features of a many-body localizable system under an actual electric field or current drive.

Note added in the manuscript – During the writing of the manuscript we became aware of ref.40 which has studied non-Hermitian MBL transition in the same model. Our focus, i.e. to study current carrying NESS, is entirely different from that of ref.40. Our results and conclusions are also substantially different from those in ref.40. In particular, unlike ref.40, we find that the phase boundaries in $W - \epsilon$ plane for \mathcal{T} reversal-symmetry breaking and entanglement transitions are distinct.

Acknowledgement: We thank Subroto Mukerjee and Abhishek Dhar for useful discussions. SB acknowledges support from The Infosys Foundation (India), and SERB (DST, India) ECR award .

[1] J. M. Deutsch, ‘‘Quantum statistical mechanics in a closed system,’’ *Phys. Rev. A* **43**, 2046–2049 (1991).
 [2] Mark Srednicki, ‘‘Chaos and quantum thermalization,’’ *Phys. Rev. E* **50**, 888–901 (1994).
 [3] Mark Srednicki, ‘‘The approach to thermal equilibrium in

quantized chaotic systems,’’ *Journal of Physics A: Mathematical and General* **32**, 1163 (1999).
 [4] E. Altman and R. Vosk, ‘‘Universal dynamics and renormalization in many-body-localized systems,’’ *Annu. Rev. Condens. Matter Phys.* **6**, 383 (2015).

- [5] R. Nandkishore and D. A. Huse, “Many-body localization and thermalization in quantum statistical mechanics,” *Annu. Rev. Condens. Matter Phys.* **6**, 15 (2015).
- [6] Dmitry A. Abanin, Ehud Altman, Immanuel Bloch, and Maksym Serbyn, “Many-body localization, thermalization, and entanglement,” arXiv e-prints , arXiv:1804.11065 (2018), [arXiv:1804.11065 \[cond-mat.dis-nn\]](#).
- [7] For an ergodic eigenstate, the entanglement entropy is equal to the thermal entropy corresponding to the energy density of the eigenstate.
- [8] Jens H. Bardarson, Frank Pollmann, and Joel E. Moore, “Unbounded growth of entanglement in models of many-body localization,” *Phys. Rev. Lett.* **109**, 017202 (2012).
- [9] Maksym Serbyn, Z. Papić, and Dmitry A. Abanin, “Universal slow growth of entanglement in interacting strongly disordered systems,” *Phys. Rev. Lett.* **110**, 260601 (2013).
- [10] Ronen Vosk and Ehud Altman, “Many-body localization in one dimension as a dynamical renormalization group fixed point,” *Phys. Rev. Lett.* **110**, 067204 (2013).
- [11] D.M. Basko, I.L. Aleiner, and B.L. Altshuler, “Metal-insulator transition in a weakly interacting many-electron system with localized single-particle states,” *Annals of Physics* **321**, 1126 – 1205 (2006).
- [12] I. V. Gornyi, A. D. Mirlin, and D. G. Polyakov, “Interacting electrons in disordered wires: Anderson localization and low- t transport,” *Phys. Rev. Lett.* **95**, 206603 (2005).
- [13] Vadim Oganesyan and David A. Huse, “Localization of interacting fermions at high temperature,” *Phys. Rev. B* **75**, 155111 (2007).
- [14] Arijeet Pal and David A. Huse, “Many-body localization phase transition,” *Phys. Rev. B* **82**, 174411 (2010).
- [15] Michael J. Gullans and David A. Huse, “Entanglement structure of current-driven diffusive fermion systems,” (2018), [arXiv:1804.00010 \[cond-mat.stat-mech\]](#).
- [16] Michael J. Gullans and David A. Huse, “Localization as an entanglement phase transition in boundary-driven Anderson models,” arXiv e-prints , arXiv:1902.00025 (2019), [arXiv:1902.00025 \[cond-mat.stat-mech\]](#).
- [17] Raghu Mahajan, C. Daniel Freeman, Sam Mumford, Norm Tubman, and Brian Swingle, “Entanglement structure of non-equilibrium steady states,” (2016), [arXiv:1608.05074 \[cond-mat.str-el\]](#).
- [18] Cristian Zanoci and Brian G. Swingle, “Entanglement and thermalization in open fermion systems,” arXiv e-prints , arXiv:1612.04840 (2016), [arXiv:1612.04840 \[cond-mat.mes-hall\]](#).
- [19] Tomaž Prosen and Marko Žnidarič, “Matrix product simulations of non-equilibrium steady states of quantum spin chains,” *Journal of Statistical Mechanics: Theory and Experiment* **2009**, P02035 (2009).
- [20] Marko Žnidarič, “Anomalous nonequilibrium current fluctuations in the heisenberg model,” *Phys. Rev. B* **90**, 115156 (2014).
- [21] Michael M. Wolf, Frank Verstraete, Matthew B. Hastings, and J. Ignacio Cirac, “Area laws in quantum systems: Mutual information and correlations,” *Phys. Rev. Lett.* **100**, 070502 (2008).
- [22] Naomichi Hatano and David R. Nelson, “Localization transitions in non-hermitian quantum mechanics,” *Phys. Rev. Lett.* **77**, 570–573 (1996).
- [23] Naomichi Hatano and David R. Nelson, “Vortex pinning and non-hermitian quantum mechanics,” *Phys. Rev. B* **56**, 8651–8673 (1997).
- [24] Naomichi Hatano and David R. Nelson, “Non-hermitian delocalization and eigenfunctions,” *Phys. Rev. B* **58**, 8384–8390 (1998).
- [25] Carl M. Bender and Stefan Boettcher, “Real spectra in non-hermitian hamiltonians having \mathcal{PT} symmetry,” *Phys. Rev. Lett.* **80**, 5243–5246 (1998).
- [26] Carl M Bender, “Making sense of non-hermitian hamiltonians,” *Reports on Progress in Physics* **70**, 947–1018 (2007).
- [27] Takahiro Fukui and Norio Kawakami, “Breakdown of the mott insulator: Exact solution of an asymmetric hubbard model,” *Phys. Rev. B* **58**, 16051–16056 (1998).
- [28] Takashi Oka and Hideo Aoki, “Dielectric breakdown in a mott insulator: Many-body schwinger-landau-zener mechanism studied with a generalized bethe ansatz,” *Phys. Rev. B* **81**, 033103 (2010).
- [29] Vikram Tripathi, Alexey Galda, Himadri Barman, and Valerii M. Vinokur, “Parity-time symmetry-breaking mechanism of dynamic mott transitions in dissipative systems,” *Phys. Rev. B* **94**, 041104 (2016).
- [30] L. D. Landau and A. M. Lifshitz, *Quantum Mechanics* (Pergamon, 1958).
- [31] A. M. Dykhne, “Adiabatic perturbation of discrete spectrum states,” *Sov. Phys. JETP* **14**, 941 (1962).
- [32] Dorje C. Brody and Eva-Maria Graefe, “Mixed-state evolution in the presence of gain and loss,” *Phys. Rev. Lett.* **109**, 230405 (2012).
- [33] David J. Luitz, Fabien Alet, and Nicolas Laflorencie, “Universal behavior beyond multifractality in quantum many-body systems,” *Phys. Rev. Lett.* **112**, 057203 (2014).
- [34] David J. Luitz, Nicolas Laflorencie, and Fabien Alet, “Many-body localization edge in the random-field heisenberg chain,” *Phys. Rev. B* **91**, 081103 (2015).
- [35] See Supplemental Material.
- [36] As in the exact diagonalization studies of standard MBL systems [34], the critical exponents extracted for the non-Hermitian model from finite-size scaling limited to such small systems does not have much importance. However, the data collapse clearly brings out the existence of the transition.
- [37] Jonas A. Kjäll, Jens H. Bardarson, and Frank Pollmann, “Many-body localization in a disordered quantum ising chain,” *Phys. Rev. Lett.* **113**, 107204 (2014).
- [38] Since the many-body spectra for the real part of the eigenvalues are exponentially dense, the actual typical level spacing $\delta_{typ} \sim e^{-L}$. However this does not contribute to the time evolution in Figs.3(a)-(c) for $t \ll e^L$.
- [39] Tankut Can, Vadim Oganesyan, Dror Orgad, and Sarang Gopalakrishnan, “Spectral gaps and mid-gap states in random quantum master equations,” arXiv e-prints , arXiv:1902.01414 (2019), [arXiv:1902.01414 \[quant-ph\]](#).
- [40] Ryusuke Hamazaki, Kohei Kawabata, and Masahito Ueda, “Non-Hermitian Many-Body Localization,” arXiv e-prints , arXiv:1811.11319 (2018), [arXiv:1811.11319 \[cond-mat.dis-nn\]](#).

Supplemental Material
for

Entanglement in non-equilibrium steady states and many-body localization breakdown through dissipative tunneling
by Animesh Panda, and Sumilan Banerjee

S1: Evolution of phase diagram as a function of Ψ

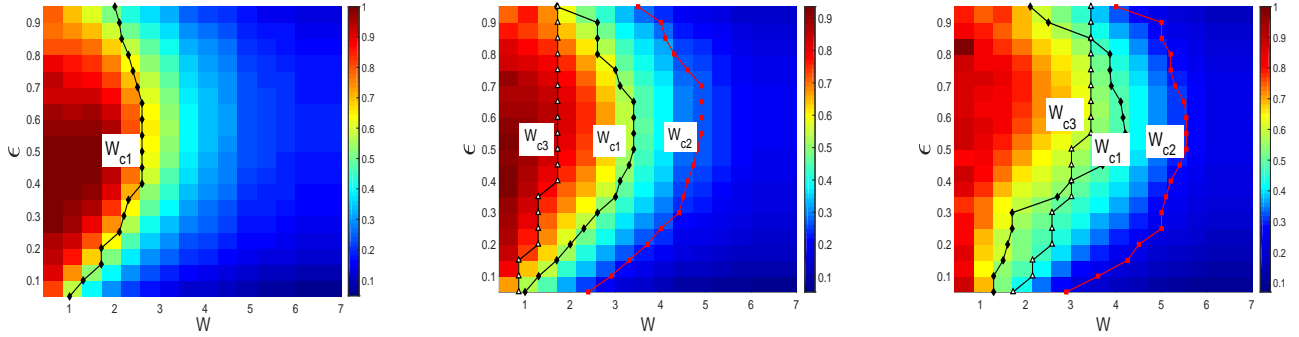


FIG. S1. **Phase diagrams:** The phase boundaries as a function of energy density ϵ (see main text) and disorder W – (i) W_{c1} , Hilbert space delocalization-localization and entanglement transitions, (ii) W_{c2} , time-reversal breaking transition, and (iii) W_{c3} , current transition (see the main text for the definitions). The values of the non-Hermitian strength are $\Psi = 0$ (left), $\Psi = 0.3$ (middle), same as Fig.1(c), and $\Psi = 0.6$ (right).

In this section we show the evolution of the phase diagram, the one shown in Fig.1(c) (main text), as a function of the strength of the non-Hermitian term Ψ [Eq.(1)]. As shown in Figs.S1, the three phase boundaries W_{c1} , W_{c2} and W_{c3} naturally shift to higher disorder with increasing Ψ . We obtain the phase boundary, $W_{c1}(\epsilon)$, from the peak of the standard deviation of entanglement entropy σ_E [Fig.2(b)]. Similar, albeit slightly higher, values for W_{c1} are obtained from the crossing of S_{EE}/L vs. W curves [Fig.2(a)(inset)]. However, we do not use the crossing point to plot phase boundary as a function of ϵ , since clear crossings can only be detected over middle one-third and one-half of the spectra for $\Psi = 0.3$ and $\Psi = 0.6$, respectively. We note that the clear crossing point for S_{EE}/L vs. W curves could be obtained for the Hermitian case ($\Psi = 0$) almost over the entire spectrum, except at the very edges.

S2: Transition from volume-law to area-law entanglement for $\Psi = 0.3$

The MBL transition is defined from volume-law to area-law transition [34] in the Hermitian case, i.e. $\Psi = 0$ in Eq. 1. A similar transition is also observed for $\Psi = 0.3$ with increasing disorder, as evident from Fig.S2(a) for $\epsilon = 0.5$. This is further corroborated by clear crossing of S_{EE}/L vs. W curves for different L in Fig.S2(b) (also shown in the inset of Fig.2(a), main text). This crossing point is used to find out the critical disorder W_{c1} .

1. Finite-size scaling collapses for different values of Ψ

In this section we show the finite-size scaling collapses, similar to the ones shown in Figs.2, for $\Psi = 0$ and $\Psi = 0.6$ at the middle of the spectrum $\epsilon = 0.5$. Fig.S3 shows the data collapses for $\Psi = 0$. The entanglement transition W_{c1} is extracted to be $\sim 3.3 \pm 0.1$. Somewhat higher values of critical disorder for the MBL transition is obtained in ref.34, which considers larger system sizes up to $L = 22$. It is a known effect in exact diagonalization studies of MBL, namely the critical disorder strength tends to shift to higher values with increasing L for the limited system sizes accessible so far.

The finite-size data collapse for $\Psi = 0.6$ is shown in Fig.S4. All the three values of the critical disorders (W_c 's) for the three transitions, and the critical exponents (ν 's) increase as we go from $\Psi = 0.3$ (Figs.2) to $\Psi = 0.6$ (Figs.S4). Surprisingly we obtain two peaks in the variance σ_E for $L = 14$ and $L = 16$ [Fig.S4(b)]. As evident, the two-peak structure becomes more prominent for the higher system size. The reason behind the two-peak structure is not clear at present and will be studied in a future work.

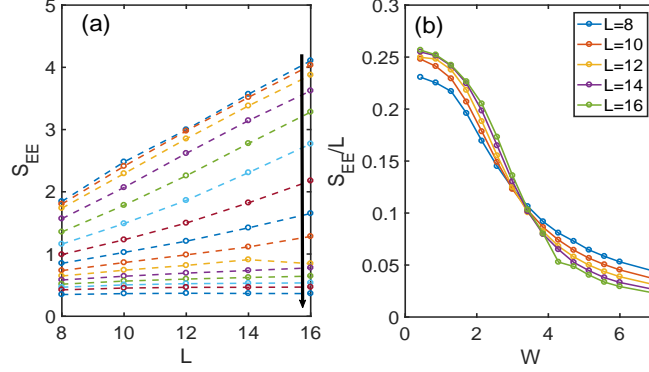


FIG. S2. **Volume-law to area-law transition for $\Psi = 0.3$:** (a) S_{EE} as function of L for different disorder strengths at $\epsilon = 0.5$; the arrow denotes the direction of increasing disorder (W), from 0.43 to 7. (b) S_{EE}/L is plotted against W for different L .

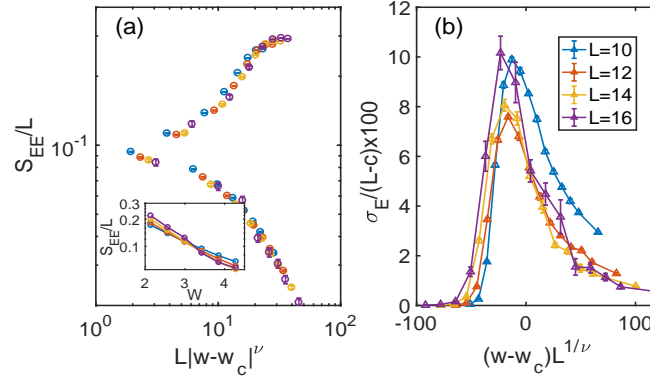


FIG. S3. **Entanglement transition for $\Psi = 0$:** (a) S_{EE}/L and (b) σ_E for $\epsilon = 0.5$. The transition is detected from the system size crossing of S_{EE}/L in the inset of (a). The values of the critical exponent and critical disorder extracted for the transition is $\nu_1 \simeq 0.8$, $W_{c1} = 3.3 \pm 0.1$.

We note that the average S_{EE} and σ_E shown in Figs. 2, S3, S4 and S2 are obtained by averaging over the eigenstates with real eigenvalues. The averaging over the eigenstates with complex eigenvalues also gives similar results.

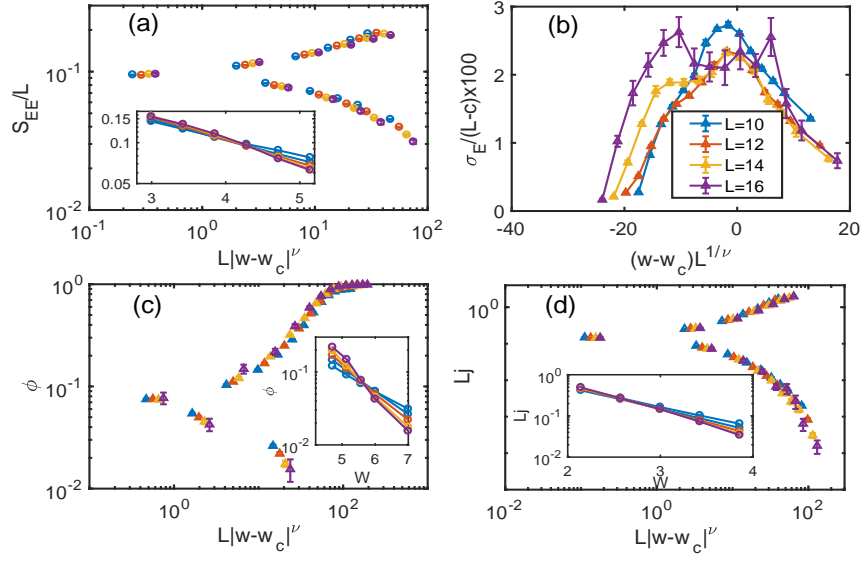


FIG. S4. **Entanglement and \mathcal{T} -reversal breaking transitions for $\Psi = 0.6$:** Data collapses for (a) S_{EE}/L , (b) σ_E , (c) ϕ and (d) Lj , at $\epsilon = 0.5$. The transitions are detected from the system size crossings shown in the insets of (a), (c) and (d). The values of the critical exponents and critical disorder extracted for the three transitions are, (a) $\nu_1 \simeq 1.5$, $W_{c1} = 4.2 \pm 0.1$, (c) $\nu_2 \simeq 1.5$, $W_{c2} = 5.6 \pm 0.1$ and (d) $\nu_3 \simeq 1.5$, $W_{c3} = 2.95 \pm 0.10$; c is a fitting parameter in (b) (see main text).

S3: Time evolution for different values of Ψ

1. Spectrum of the Liouvillian operator

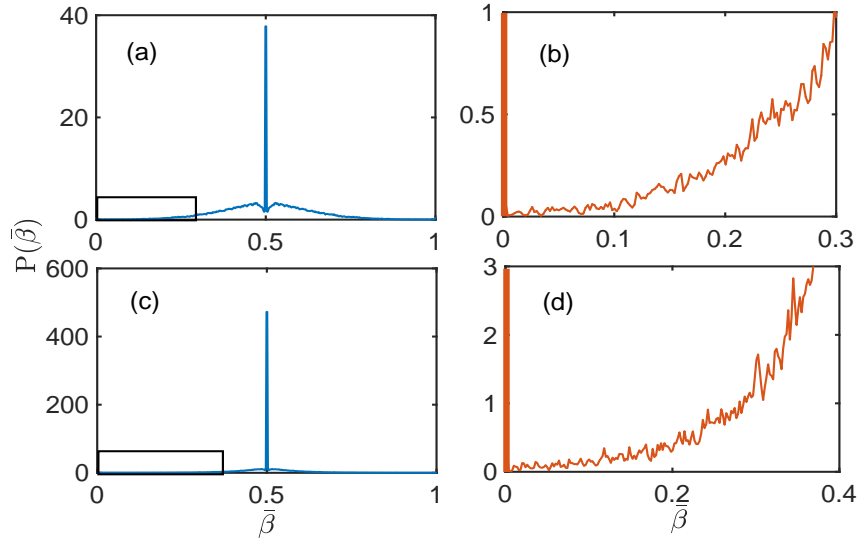


FIG. S5. **Probability distribution of the real part of the eigenvalues of the Liouvillian operator:** The probability distribution $P(\bar{\beta})$ for (a) $W = 1$ and (b) $W = 2$ for $\Psi = 0.3$. The boxes in (a) and (c) highlight the gapped part of the spectra, which are zoomed in (b) and (d), respectively.

As discussed in the main text, the time evolution of the density matrix is controlled by the eigenspectrum of the Liouvillian operator \mathcal{L} in Eq.(2). The relaxation of the system to the NESS is controlled by the real part of the

eigenvalues of \mathcal{L} , i.e. $-\beta_{nm} > 0$, where $\beta_{nm} = 2\Lambda_s - \Lambda_n - \Lambda_m$. In Figs.S5, we plot the disorder averaged distribution, $P(\bar{\beta})$, of the normalized quantity, $\bar{\beta} = (\beta - \beta_0)/(\beta_M - \beta_0)$ for $\Psi = 0.3$. Here β_0 and β_M are the minimum and the maximum values of β_{nm} , respectively. Since the imaginary eigenvalues of the non-Hermitian Hamiltonian in Eq.(1) appears in complex conjugate pairs, the probability distribution is symmetric about $\bar{\beta} = 1/2$. Also, there is a peak at $\bar{\beta} = 0$, which corresponds to the NESS, as mentioned in the main text. As shown in Figs.S5, the peak is separated from most of the spectrum by a long tail. In the limit $L \rightarrow \infty$, the tail is expected to tend to a gap, β_g , that separates the peak from the relaxation modes with $\bar{\beta} > 0$.

2. Entanglement entropy of NESS

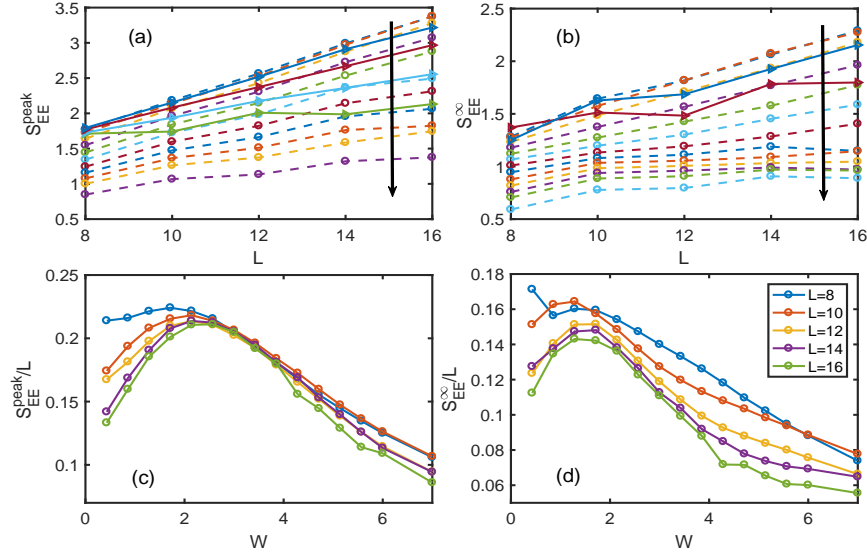


FIG. S6. S_{EE}^{peak} and S_{EE}^{∞} for $\Psi = 0.3$: (a) S_{EE}^{peak} and (b) S_{EE}^{∞} as a function of L for different W . The solid and dashed lines in (a) and (b) are for $W < W_m$ and $W > W_m$, respectively; $W_m = 2$ in (a) and $W_m = 1.2$ in (b) are the positions of the maxima in S_{EE}^{peak} and S_{EE}^{∞} , respectively, as function of W . In (a) and (b) the arrows indicate the direction of increasing W for the dashed lines and direction of decreasing W for the solid lines. The range of W is from 0.43 to 7. As shown in (c) and (d) unlike average S_{EE}/L , S_{EE}^{peak}/L and S_{EE}^{∞}/L do not show any crossing when plotted against W .

In this section we study S_{EE}^{∞} , as well as the maximum value of $S_{EE}(t)$, i.e. S_{EE}^{peak} [Figs.3(a)-(c)], as a function of W and L . For a given L , unlike the eigenstate averaged S_{EE} [Fig.S2(a), the maxima in S_{EE}^{peak} and S_{EE}^{∞} appear at a finite disorder, as shown in Figs.S6(a)-(d). Also, we do not see any system-size crossing for S_{EE}^{∞}/L (S_{EE}^{peak}/L) vs. W in Fig.S6(c)(Fig.S6(d)). We were also not able to obtain any finite-size data collapse for S_{EE}^{∞} and S_{EE}^{peak} .

3. Time evolution of Ne'el order parameter

As discussed in the main text, we characterize the memory of the initial state by the Ne'el order parameter $N(t)$. For the Hermitian case $\Psi = 0$, as shown in Fig.S7(a) for $W = 0.43 < W_{c1}$, the long-time value N_{∞} goes to zero in the ergodic phase. This can be seen from the fact that N_{∞} decreases with L tending to zero for $L \rightarrow \infty$. On the contrary, in the MBL phase, for $W = 4.3, 7$, N_{∞} approaches a constant value with increasing L . Hence, the Ne'el order parameter in this case serves as the MBL order parameter, i.e. it diagnoses the persistence of the initial memory at arbitrary long times. In the non-Hermitian model [Eq.(1)], the NESS is approached at long times. This is true even deep in the MBL phase, $W \gg W_{c2}$, since there is always a finite number of eigenstates with complex eigenvalues, albeit with a vanishing fraction, for any finite-size system. Of course, for $W \gg W_{c2}$, it is expected that the imaginary part of the eigenvalues $\sim e^{-L/\zeta}$, and, hence, the NESS will ensue only after a very long time $\sim e^{L/\zeta}$ for large systems. As shown in Fig.S7(b) for $\Psi = 0.6$, and in Fig.3(f) for $\Psi = 0.3$, the Ne'el order parameter for the NESS decreases rapidly with L , presumably approaching zero for $L \rightarrow \infty$. However, as mentioned in the main text,

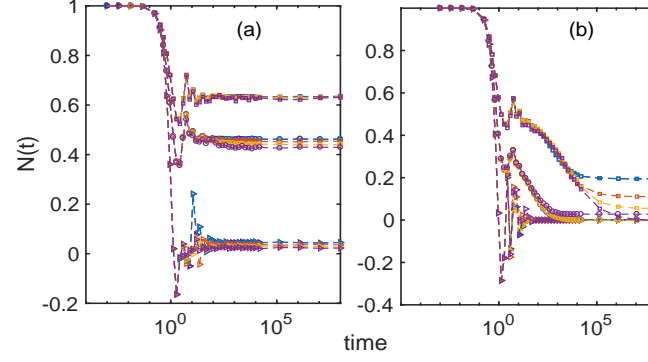


FIG. S7. **Time evolution of Neel order parameter:** The Neel order parameter $N(t)$ is shown for (a), the Hermitian case, $\Psi = 0$, and (b) $\Psi = 0.6$, as a function of W and L . The triangles, circles and squares are for $W = 0.43, 4.3, 7$ respectively, with $L = 10$ (blue), $L = 12$ (orange), $L = 14$ (yellow) and $L = 16$ (purple).

there is an interesting dynamical regime $\beta_{typ}^{-1} < t < \beta_g^{-1}$ over which $N(t)$ tends to plateau, retaining the memory of the initial state.